High-Resolution Simulations of Wintertime Precipitation in the Colorado Headwaters Region: Sensitivity to Physics Parameterizations

CHANGHAI LIU, KYOKO IKEDA, GREGORY THOMPSON, ROY RASMUSSEN, AND JIMY DUDHIA

National Center for Atmospheric Research, Boulder, Colorado*

(Manuscript received 4 January 2011, in final form 26 April 2011)

ABSTRACT

An investigation was conducted on the effects of various physics parameterizations on wintertime precipitation predictions using a high-resolution regional climate model. The objective was to evaluate the sensitivity of cold-season mountainous snowfall to cloud microphysics schemes, planetary boundary layer (PBL) schemes, land surface schemes, and radiative transfer schemes at a 4-km grid spacing applicable to the next generation of regional climate models.

The results indicated that orographically enhanced precipitation was highly sensitive to cloud microphysics parameterizations. Of the tested 7 parameterizations, 2 schemes clearly outperformed the others that overpredicted the snowfall amount by as much as ~30%–60% on the basis of snow telemetry observations. Significant differences among these schemes were apparent in domain averages, spatial distributions of hydrometeors, latent heating profiles, and cloud fields. In comparison, model results showed relatively weak dependency on the land surface, PBL, and radiation schemes, roughly in the order of decreasing level of sensitivity.

1. Introduction

Quantitative orographic precipitation has been a vexing problem in both numerical weather prediction (NWP) models and regional climate models (e.g., Colle et al. 1999; Leung and Qian 2003). As demonstrated by the overall better performance at higher resolutions in previous sensitivity studies (e.g., Colle et al. 1999; Colle and Mass 2000; Leung and Qian 2003), inadequate terrain representation is commonly believed to be a major impediment for improving the poor skill of NWP and regional climate models. Some detailed case studies of high-impact winter storms in complex terrain showed that a grid spacing close to 1 km sufficiently captures the complex mesoscale forcings related to terrain features (Garvert et al. 2005; Colle et al. 2008). A recent regional climate modeling study (Ikeda et al. 2010; Rasmussen et al. 2011) suggested that reasonable seasonal snowfall simulations over the topographically diverse Colorado region could be achieved with grid spacings at 6 km or below.

In spite of the strikingly positive impact, however, resolution enhancement alone may not meet the challenging difficulties in orographic precipitation simulations. For instance, Colle et al. (2000) noted significant overprediction of wintertime precipitation over the upper windward slopes and underprediction in the lowlands at 4 km spacing, whereas Garvert et al. (2005) reported apparent precipitation overprediction at both the windward and lee sides with 1.33-km spacing. An overestimation of precipitation on both sides of the higher barriers was also documented at comparable horizontal resolutions by Grubišić et al. (2005), and the poor skill was not improved by increasing the horizontal resolutions. These results strongly suggest that as well as the use of high resolutions, adequate treatments of cloud microphysics and subgrid processes in numerical models are also critical to skillful simulations of topographic precipitation.

The impacts of cloud microphysics on orographic precipitation have been addressed through both idealized two-dimensional and real-data simulations. Idealized studies mostly focused on the effects of the uncertainties in the microphysical parameters and showed considerable variations in precipitation amount

* The National Center for Atmospheric Research is sponsored by the National Science Foundation.

Corresponding author address: Dr. Changhai Liu, National Center for Atmospheric Research, P. O. Box 3000, Boulder, CO 80307-3000.
E-mail: chliu@ucar.edu

DOI: 10.1175/MWR-D-11-00009.1

and hydrometeor distributions in response to changes in some parameters (cf. Thompson et al. 2004). In an observed case investigation using a mesoscale numerical model, Reisner et al. (1998) evaluated three options of increasing complexity to represent the hydrometeor species (viz., two-class ice, three-class ice predicting mass only, and three-class ice predicting mass and number) in predicting supercooled liquid water within winter storms. Comparisons of the simulations to observations showed that the most sophisticated double-moment scheme produced the best forecast in that case. Colle and Mass (2000) compared the 24-h precipitation amounts from five microphysical schemes of varying complexity for a flooding event over the Pacific Northwest. They found that the warm rain scheme generated too much precipitation along the windward slopes, but the most sophisticated scheme did not necessarily produce more accurate forecasts. Grubišić et al. (2005) explored the dependence of wintertime heavy orographic precipitation predictions in the Sierra Nevada on the choice of microphysical parameterizations and showed fairly low skill with excessive overprediction consistently among the four schemes tested. Jankov et al. (2007, 2009) analyzed the performance of a high-resolution numerical model using four different microphysics schemes for several ''atmospheric river'' rainfall events during a winter season in northern California and noted a large sensitivity to changes in microphysics. Milbrandt et al. (2010) found that the leeside precipitation overprediction in some previous studies (e.g., Garvert et al. 2005) was correctable through details in the microphysics, and they also reported a great sensitivity in both precipitation and hydrometeor mass fields to the number of predicted moments in a bulk microphysics scheme.

In contrast to the microphysics sensitivity, little is known about how the orographic precipitation could be affected by the selection of other subgrid parameterizations, such as land surface models (LSMs), planetary boundary layer (PBL) schemes, and radiation transfer models. Without question, a systematic quantification of these processes is needed, even though it is generally believed that they are less important in the winter than in the summer due to the weak energy exchanges between the surface and overlying atmosphere, shallow PBLs, and weak solar heating.

The present study focuses on the wintertime precipitation over the Colorado Headwaters region because of the effects of complex terrain, abundant snowfall amount, and its significance as a regional water resource. In addition, a relatively dense snow-telemetry network facilitates the verification of model results. Herein, our principal objective was to evaluate the dependency of quantitative winter season snowfall simulations on various physics parameterizations in high-resolution regional climate models. A unique aspect of our simulations is the seasonal integration at fine horizontal resolution, in contrast to previous fine-grid but short-term simulations of the numerical weather prediction type or long-term but coarse-grid regional climate simulations. Therefore, a particular strength of this research is that the results are robust enough to report fully systematic biases of various microphysical schemes, unlike prior works that draw rather weak conclusions based on too few datasets. Note that the utilization of high resolution eliminates the complication of traditional cumulus parameterizations in the interpretation of model results, and this is an additional benefit as well as a critical requirement of adequate representation of underlying topography. The results will provide useful guidance for the regional climate community to make an appropriate selection of a set of physical parameterizations and suggestions on which physics processes may require further improvement.

The paper is organized as follows. The next section describes the configuration of the high-resolution regional climate model and the design of our numerical experiments. In section 3, the model performance and its dependency on the choice of cloud microphysics, PBL, LSM, and radiation parameterizations are examined in detail in terms of spatial and temporal precipitation distributions, cloud properties, and latent heating patterns. The paper concludes with a summary of our findings in section 4.

2. Numerical model and experiment design

In this study, version 3.1.1 of the Advanced Research Weather Research and Forecasting model (ARW-WRF; Skamarock et al. 2008) was configured into a regional climate model with a single computational domain of 1240×1040 km^2 centered at the Colorado Headwaters (Fig. 1). A horizontal grid increment of 4 km was used along with 45 stretched vertical levels and model top at 100 hPa. The selected resolution was based on our previous resolution-dependence testing that showed accurate seasonal snowfall simulations in complex terrains could be achieved with horizontal grid spacing below 6 km (Ikeda et al. 2010; Rasmussen et al. 2011). The present results confirm the similarities between simulations with 2- and 4-km spacing.

ARW-WRF offers many physical parameterizations, greatly facilitating parameterization sensitivity studies. Table 1 summarizes the sensitivity experiments, consisting of 16 experiments with different combinations of various physics parameterizations. The control simulation (CTRL) used the Thompson et al. (2008) mixed-phase microphysics scheme, the Mellor–Yamada–Janjic planetary boundary layer scheme (Janjic 2002), the Noah land surface model (Chen and Dudhia 2001), and the National Center for

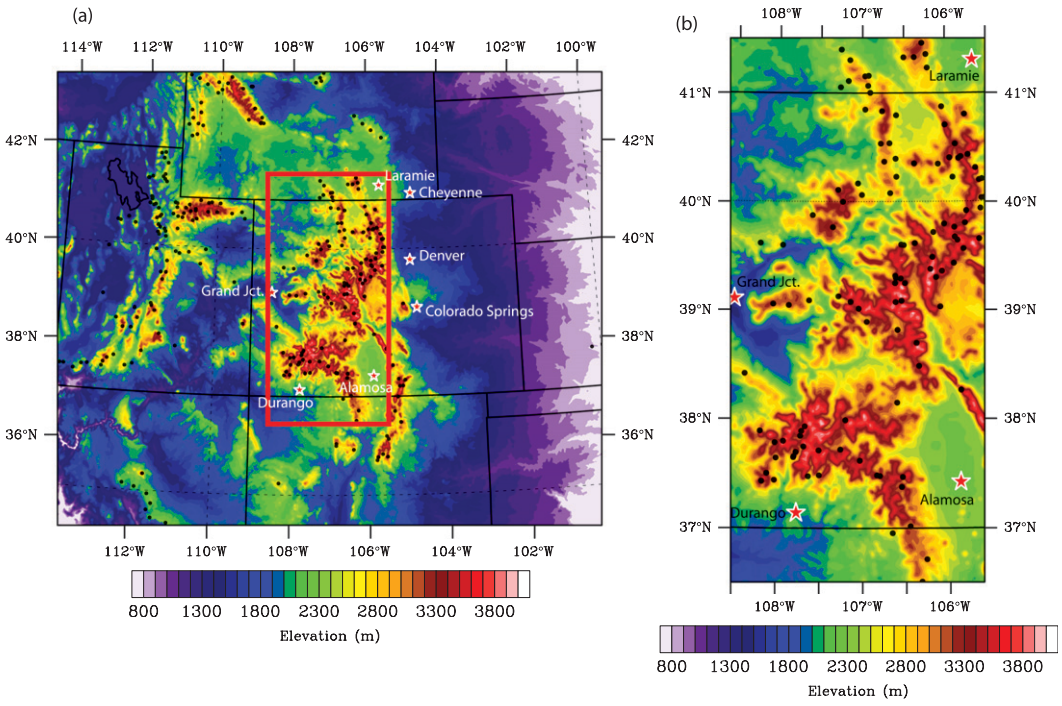

FIG. 1. Terrain of the (a) model domain and (b) the subdomain over the Colorado Headwaters region. The locations of SNOTEL sites are indicated with black dots.

Atmospheric Research (NCAR) Community Atmosphere Model (CAM) radiative transfer parameterization (Collins et al. 2004). This set of parameterization schemes for cloud microphysics, planetary boundary layer physics, land surface processes, and short- and longwave radiation was identical to those used in the studies by Ikeda et al. (2010) and Rasmussen et al. (2011). The sensitivity experiments were divided into four groups: a series of six microphysics (MP) experiments, a series of three land surface (LS) experiments, a series of five boundary layer (BL) experiments, and a single radiation sensitivity experiment. A 17th experiment, omitted from the table, used the same physics options as CTRL but reduced the grid spacing from 4 to 2 km. Unlike the previous studies by Ikeda et al. (2010) and Rasmussen et al. (2011), which simulated four full-winter seasons, these experiments focused on a very active three-month subset of one winter season during 1 December 2007–29 February 2008. The 3-hourly, 32-km grid spacing North American Regional Reanalysis (NARR) data (Mesinger et al. 2006) provided the initial and lateral boundary conditions for our numerical experiments.

3. Results

In this section, results of the CTRL simulation are compared against snowpack telemetry (SNOTEL) data (Serreze et al. 1999) and against the simulation with 2-km grid spacing. The results of the physical parameterization sensitivity experiments are then presented following the order given in Table 1.

SNOTEL sites, which are owned and operated by the Department of Agriculture Natural Resource Conservation Service (NRCS), are typically located at elevations between 2400 and 3600 m above mean sea level. They provide a long-term record of precipitation from weighing all-weather precipitation gauges throughout the western United States. Observations from 112 SNOTEL sites in the subdomain were used to compare with the model results. It should be pointed out that the undercatch due to wind is the main issue with weighing-type gauges for snowfall estimation (Serreze et al. 2001; Yang et al. 1998; Rasmussen et al. 2001). Based on the location of SNOTEL gauges in a forest clearing, most of the time, the wind speed is less than 2 m s^{-1}, for which an undercatch of approximately 10%–15% is expected (Yang et al. 1998).

a. CTRL simulation

The simulated 3-month precipitation totals shown in Fig. 2 reveal the expected correlation with topography (light gray contours). Under the predominant westerly flow, the effect of upslope mechanical lifting is obvious with precipitation maxima located on westward-facing

TABLE 1. List of numerical experiments with various physics parameterizations.

	Microphysics							Land surface		
Expt	Thompson 2-moment	Morrison 2-moment	WSM 5-class	WSM 6-class	ARW-WRF double moment 6-class	Goddard GCE	Purdue–Lin	Unified Noah	Rapid Update Cycle (RUC)	Pleim–Xiu scheme
CTRL	×							×		
MPM2M		×						×		
MPWSM5			×					×		
MPWSM6				×				×		
MPWDM6					×			×		
MPGCE						×		×		
MPLIN							×	×		
LSRUC	×								×	
LSPX	×									×
LSPX2	×									×
BLYSU	×							×		
BLQNSE	×							×		
BLMYNN	×							×		
BLMYNN3	×							×		
BLBL	×							×		
RRTMG	×							×		

slopes and mountain peaks and with far lower amounts in the valleys and east of the Rocky Mountains. SNOTEL sites, typically located at altitudes above 2500 m, are shown in Fig. 2c and exhibit a similar pattern of larger precipitation amounts at high altitudes and on westward-facing slopes.

The correspondence between model and observed precipitation is more readily discerned by plotting the average of all SNOTEL sites as found in Fig. 3. To calculate the average amount predicted by ARW-WRF, the four grid points nearest to a SNOTEL site were inverse distance weighted. Calculations performed with 4-point average, cubic, and bilinear interpolation techniques produced negligibly different results. Figure 3 also shows that the simulated average precipitation is nearly identical at 2- and 4-km grid spacing. By the end of the 3-month period, ARW-WRF overpredicts the average precipitation by approximately 6%, which is easily within known errors of the SNOTEL observational data (Yang et al. 1998). Upon closer inspection, the largest discrepancy between model and observations occurs during two events in January. Each of these cases contained very high-speed low-level winds, and we suspect that many SNOTEL sites received less snow than adjacent regions due to blowing and drifting snow. As will be shown in section 3b, all of the sensitivity experiments responded similarly during these two events with model predictions of precipitation greater than observations.

In summary, the control simulation produced a highly accurate 3-month precipitation forecast in the Colorado Headwaters region. This performance, as well as the negligible difference from the higher-resolution (2 km) simulation, justifies the experiment design for parameterization sensitivity studies.

b. Sensitivity to cloud microphysics

Among the bulk cloud physics parameterizations available in version 3.1.1 of the ARW-WRF model, seven relatively sophisticated schemes suitable for high-resolution explicit (cloud resolving) simulations were adopted for our sensitivity evaluation: (i) the Thompson et al. (2008) scheme (THOM) with recently added double-moment rain, (ii) the Purdue–Lin scheme (PLIN; Chen and Sun 2002) based on Lin et al. (1983), (iii) the WRF Single-Moment 5-Class Scheme (WSM5; Hong and Lim 2006), (iv) the WRF Single-Moment 6-Class Scheme (WSM6; Hong and Lim 2006), (v) the Goddard cumulus ensemble model scheme (GCE; Tao and Simpson 1993), (vi) the Morrison et al. (2009) two-moment scheme (M2M), and (vii) the WRF Double-Moment 6-Class Scheme (WDM6; Lim and Hong 2010). These schemes are utilized, respectively, in experiments CTRL, MPLIN, MPWSM5, MPWSM6, MPGCE, MPM2M, and MPWDM6 (see Table 1). Most of these parameterizations contain six species of water: vapor, cloud droplets, cloud ice, rain, snow, and graupel/hail. An exception is WSM5, which excludes the graupel category. In the proceeding subsections, the effects of various cloud microphysics treatments on the seasonal simulations will be quantified through comparing the statistics of precipitation features, hydrometeors and cloud distributions, and phase-change-induced heating profiles.

TABLE 1. (*Continued*)

Surface layer					Boundary layer							Radiation	
Monin–Obukhov	Monin–Obukhov (Janjic ETA)	Pleim–Xiu	QNSE	MYNN	Mellor–Yamada (Janjic Eta)	YSU	QNSE	ACM2 (Pleim)	MYNN 2.5 level TKE	MYNN 3rd level TKE	Bougeault and Lacarrere TKE	CAM	RRTMG
	×				×							×	
	×				×							×	
	×				×							×	
	×				×							×	
	×				×							×	
	×				×							×	
	×				×							×	
	×				×							×	
	×				×							×	
		×						×				×	
×						×						×	
			×				×					×	
				×					×			×	
				×						×		×	
	×										×	×	
	×				×								×

1) TEMPORAL PRECIPITATION PATTERNS

Figure 4 compares the daily precipitation in the MP-series simulations with SNOTEL observations, all representing averages at the SNOTEL sites. Overall, all simulations generate similar temporal fluctuations that are in good agreement with observations. In particular, the heavy snowfall associated with the major winter storms around 2 and 7 December, and 5 January are clearly evident in all of the microphysics schemes. A common discrepancy is the too-heavy snowfall amounts as compared to the SNOTEL data. This deficiency is especially problematic for the PLIN parameterization, and to somewhat lesser degree, for the three W series (i.e., WSM5, WSM6, and WDM6) and GCE parameterizations, which consistently overpredict the daily amount throughout most of the 3-month integration. The underprediction happens rarely in light snowfall periods. The largest bias usually occurs when the strongest winter storms arrive in the region. Apparently, THOM and M2M outperform the others, and they almost perfectly capture the observed daily oscillation features despite the overestimates during a few major events in each month. The RMSE for THOM, M2M, WSM5, WSM6, WDM6, GCE, and PLIN is 3.0, 2.7, 3.4, 3.5, 3.5, 3.3, and 4.6 mm, respectively. In terms of the standard deviations, all parameterizations overproduce the daily precipitation variability, and again THOM and M2M are slightly superior.

Figure 5a presents the temporal variations of both modeled and observed accumulated precipitation averaged at SNOTEL sites. The accumulation is consistently overforecasted no matter what cloud microphysics scheme is applied, consistent with the daily time series in Fig. 4. The progressively divergent evolution reflects the accumulated excessive precipitation bias in the model. Evidently, THOM and M2M parameterizations share a nearly equal skill in simulating the snowfall accumulation with a few overestimates coming from the largest events in each month. The almost overlapping curves from experiments MPWSM5, MPWSM6, MPWDM6, and MPGCE with a ~28.7%–30.3% bias are less skillful than the MPTHOM and MPM2M experiments with a ~6% bias, while the MPLIN experiment has the highest precipitation bias of 56.7%. When average precipitation is calculated for the subdomain and full domain (Figs. 5b,c), then the same basic temporal and bias patterns appear between the various schemes. Also apparent in Fig. 5 and by statistics shown in Table 2, the THOM and M2M schemes produce nearly identical results, the WSM5, WSM6, WDM6, and GCE schemes produce extremely similar results to each other that have approximately 22% greater precipitation than CTRL, and the PLIN scheme produces far greater precipitation than any other scheme.

2) SPATIAL PRECIPITATION PATTERNS

The precipitation totals in all simulations display very similar regional distributions, characteristic of the topography shown previously in Fig. 2, and, thus, the broad patterns are generally insensitive to microphysics parameterizations. This weak sensitivity is consistent with the notion that, as well as the synoptic forcing, the terrain upslope lifting is the dominant process in determining orographic cloud and precipitation development in the

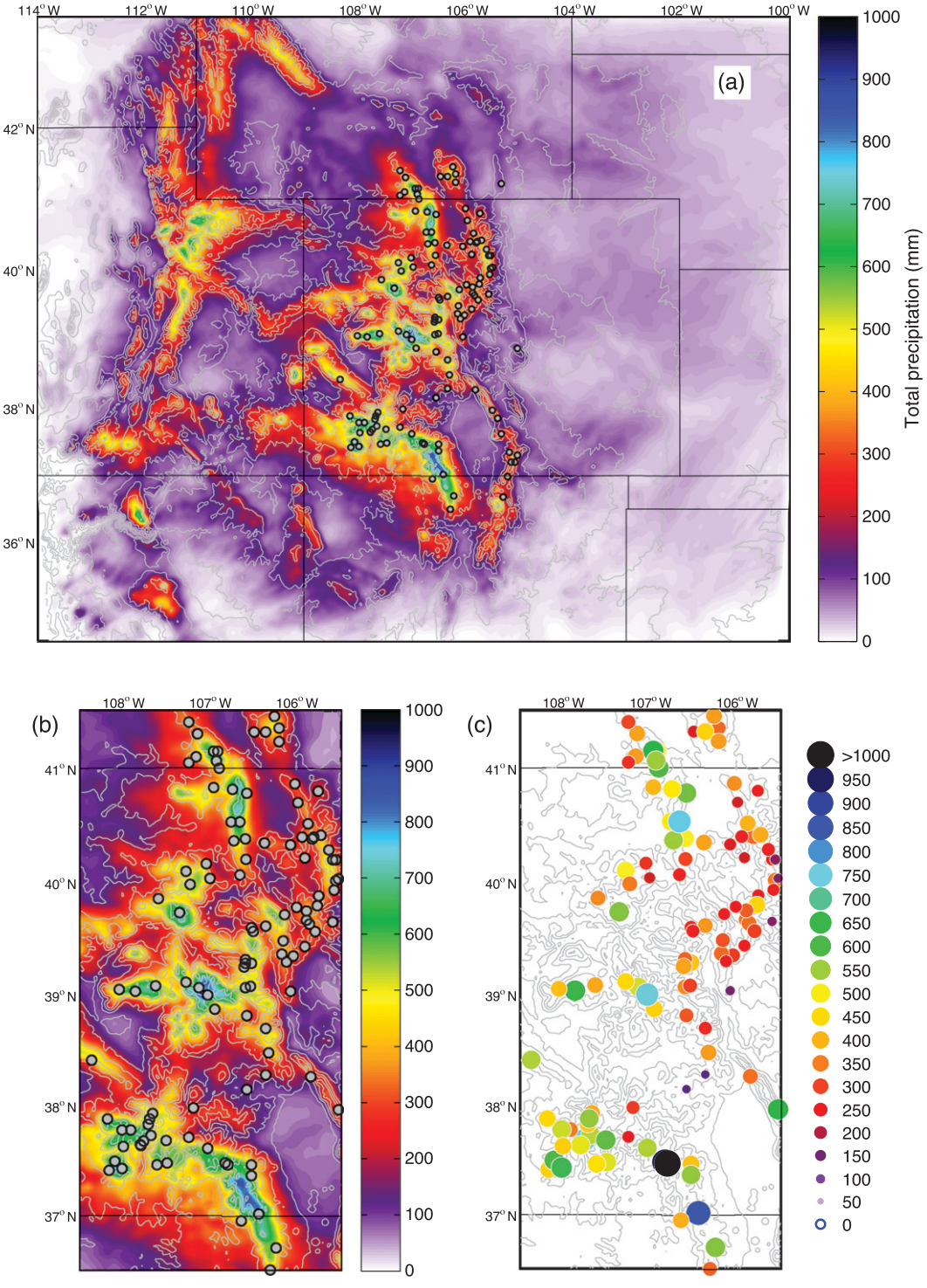

FIG. 2. Spatial distributions of the 3-month total precipitation (mm) from the CTRL simulation over (a) the full domain and (b) the subdomain. (c) The 3-month total precipitation (mm) from the SNOTEL observations (112 sites).

weakly convective wintertime environment. Therefore, a proper representation of terrain through the use of fine resolution is critical to modeling wintertime orographic precipitation in this region. Nevertheless, microphysics treatments do exert an important influence on the regional details, especially valley–ridge snowfall contrasts. Figure 6 details the spatial distributions of differential precipitation amount relative to CTRL. The largest differences

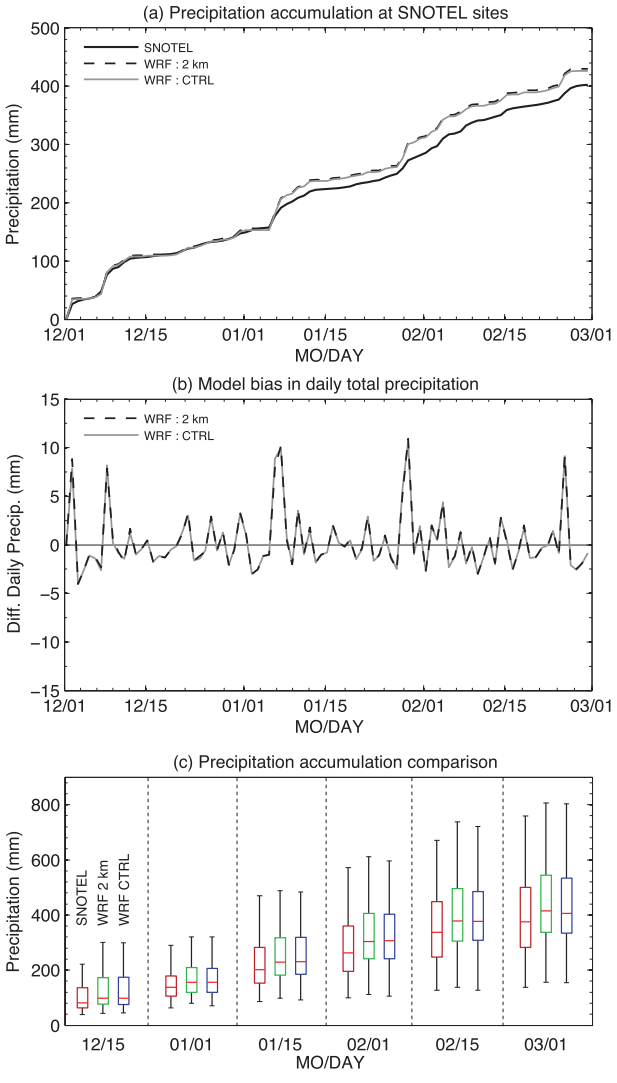

FIG. 3. (a) Comparison of average precipitation accumulation at the SNOTEL sites, CTRL, and 2-km resolution simulation. (b) Mean bias in daily precipitation between the model and the observations. (c) Boxplots showing distributions of accumulative precipitation amount for 112 SNOTEL sites and model values at SNOTEL sites on the days shown on the *x* axis. Red horizontal bars indicate the median value. The top and bottom of the boxes represent 25th and 75th percentiles of the associated data, respectively. The end points of the bottom and top whiskers are the value of the 5th and 95th percentiles, respectively.

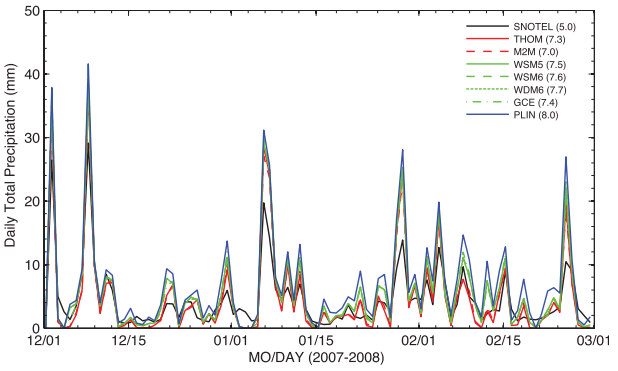

FIG. 4. Daily precipitation averaged over the SNOTEL sites for the SNOTEL data and simulations using various cloud microphysics schemes. Values in parentheses are the standard deviations of daily precipitation over the 3-month period.

are present in the areas with the steepest terrain, whereas the precipitation is more comparable east of the Rockies and also over the area between the Colorado Rockies and Utah Wasatch Range in these simulations. As expected from the earlier comparison of temporal variations, MPM2M is very close to CTRL in regional patterns, even though differences can still reach more than 50 mm at several isolated sites (Fig. 6a). In comparison with CTRL, MPM2M produces heavier snowfall along the Wasatch Range and western Colorado Rockies and lighter snowfall in the Front Range, eastern Utah, and northern Arizona.

The W-series experiments display many similarities to each other and mostly produce larger precipitation maxima than CTRL (Figs. 6b–d). The most striking feature is the excess precipitation near the western domain border, which is the first upslope region encountered by the predominant westerly winds. Apparently, the W-series microphysics schemes have a precipitation efficiency that is higher than the Thompson et al. (2008) scheme, because the CTRL experiment produces greater precipitation on the lee side of nearly all major mountain ridges. Results from the MPGCE experiment show miniscule regions where there is more precipitation predicted by CTRL (Fig. 6e). In contrast to the W-series microphysics, the GCE scheme produces slightly less upslope snow and carries more to the lee side. As further confirmation that experiment MPLIN produces the most total precipitation, Fig. 6f reveals largest extrema of precipitation differences from experiment CTRL. Similar to the W-series experiments, MPLIN has maximum differences on the windward slopes and extreme opposites in the lee of all major mountain ridges. Speculation on the causes and physical treatments within the schemes will be provided later in the paper.

The statistics of precipitation amount versus elevation in Fig. 7 further reveal some effects of cloud microphysics on spatial patterns. A positive correlation between precipitation amount and terrain height is noticeable in all simulations as indicated by the fitted curves. The variation or scatter in precipitation amount increases with elevation. While MPLIN shows the largest scatter for the highest elevations, MPTHOM, MPM2M, and MPGCE produce relatively less scatter as elevation increases.

Table 2 presents the precipitation totals averaged over the SNOTEL sites, the Colorado Headwaters area, and the entire domain. The sensitivity due to choice of

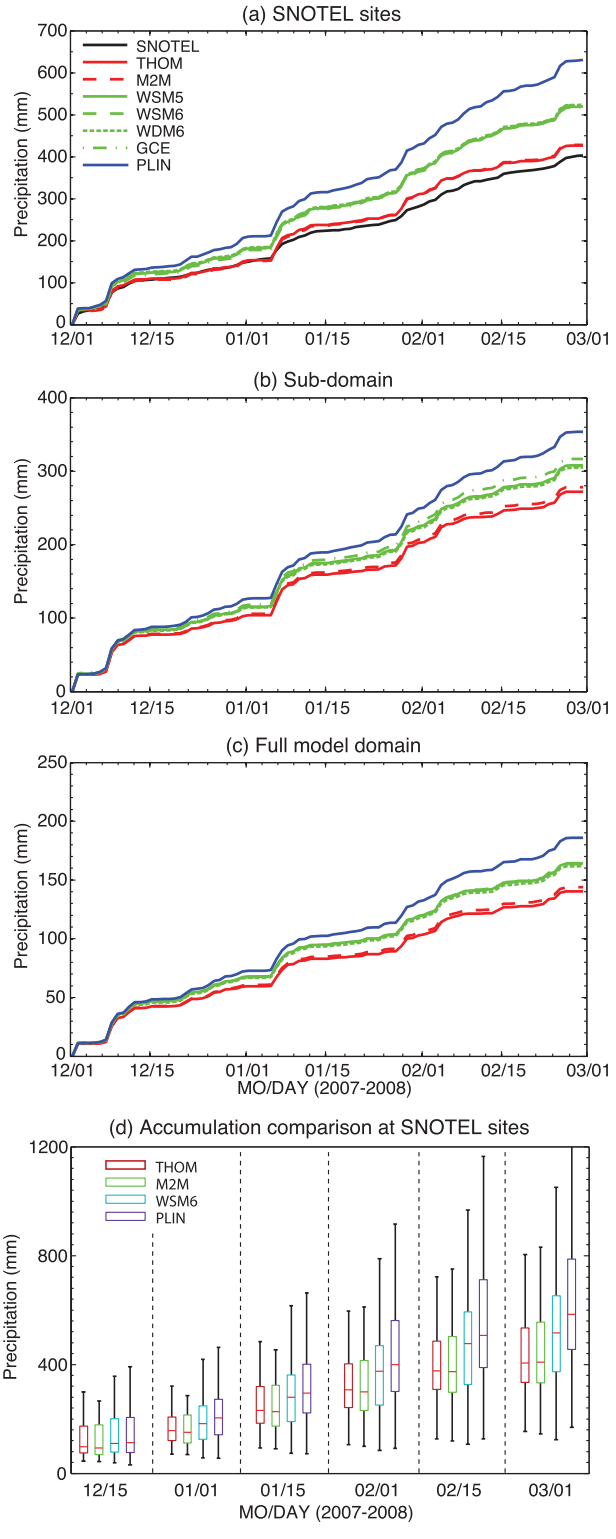

FIG. 5. Evolution of accumulated precipitation averaged over (a) the SNOTEL sites, (b) the subdomain, and (c) the full model domain for simulations using various microphysical parameterizations. (d) Boxplot of model precipitation accumulation averaged over the 112 SNOTEL sites using THOM, M2M, WSM6, and PLIN schemes.

TABLE 2. Comparison of 3-month precipitation total (mm) averaged over the model domain, subdomain, and SNOTEL sites in simulations using various physics parameterizations.

	CTRL	MPM2M	MPWSM5	MPWSM6	MPWDM6	MPGCE	MPLIN	LSRUC	LSPX	LSPX2	BLYSU	BLQNSE	BLMYNN	BLMYNN3	BLBL	RRTMG
SNOTEL avg (mm)	426.2	428.3	520.1	523.6	524.7	518.4	630.9	445.4	462.6	479.6	424.8	436.5	428.4	428.2	427.9	415.0
Bias from obs (%)	5.8	6.4	29.2	30.0	30.3	28.7	56.7	10.6	14.8	19.0	5.4	8.3	6.3	6.2	6.2	3.0
Diff from CTRL (%)	N/A	0.5	21.9	22.7	22.9	21.5	48.0	4.4	8.5	12.4	−0.4	2.3	0.4	0.4	0.3	−2.7
Subdomain avg (mm)	282.4	288.8	319.0	318.0	315.9	327.4	365.0	295.7	300.8	308.5	282.7	288.1	285.3	285.0	289.2	279.1
Diff from CTRL (%)	N/A	2.3	13.0	12.6	11.9	15.9	29.2	4.7	6.5	9.2	0.1	2.0	1.0	0.9	2.4	−1.2
Domain avg (mm)	145.7	149.2	169.8	169.1	167.3	169.7	191.8	152.9	154.3	156.3	149.8	146.8	146.8	146.7	156.1	145.8
Diff from CTRL (%)	N/A	2.4	16.6	16.1	14.8	16.5	31.7	5.0	5.9	7.3	2.9	0.8	0.8	0.7	7.1	0.1

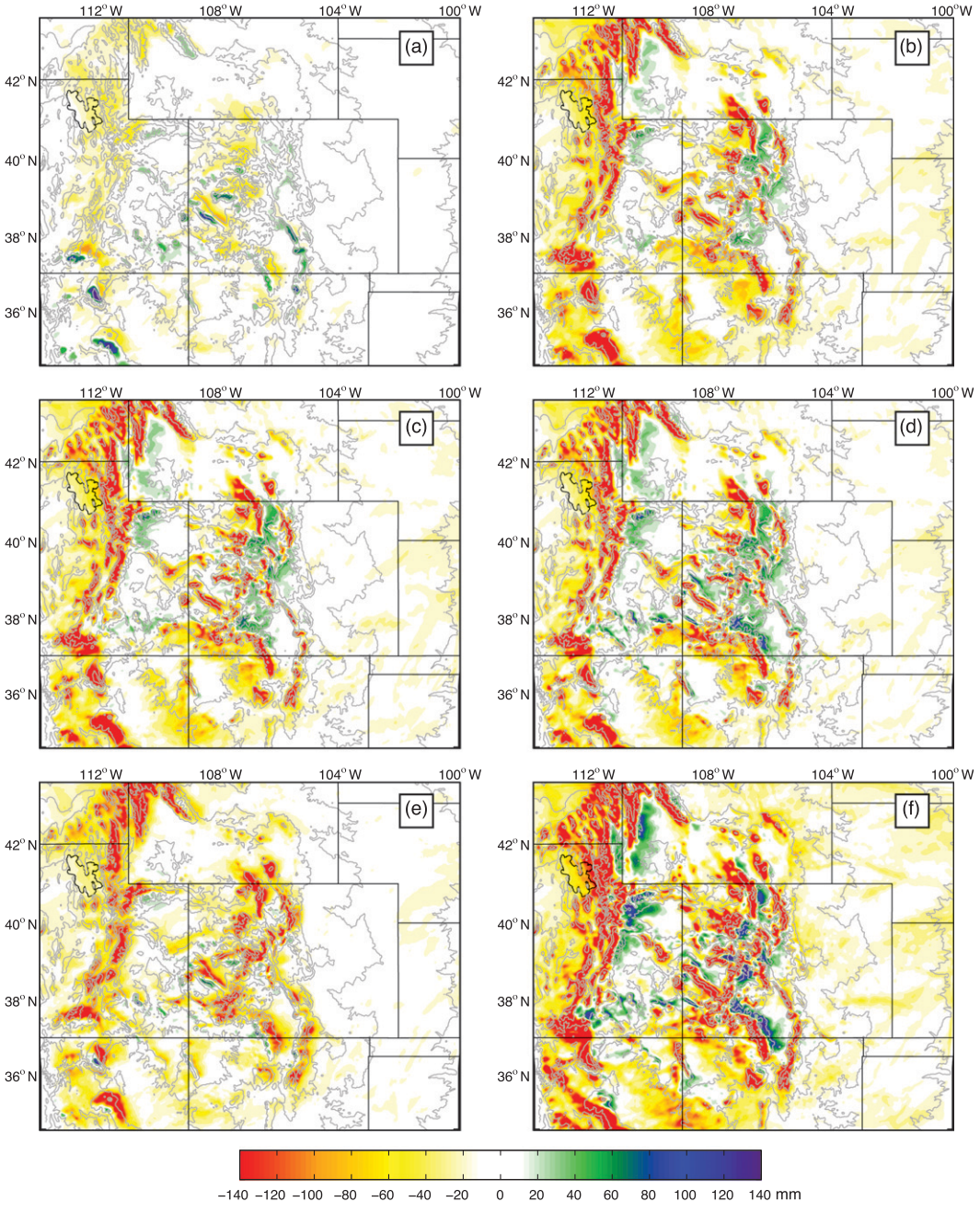

FIG. 6. Differential accumulated precipitation between CTRL and various microphysics schemes: (a) CTRL − MPM2M, (b) CTRL − MPWSM5, (c) CTRL − MPWSM6, (d) CTRL − MPWDM6, (e) CTRL − MPGCE, and (f) CTRL − MPLIN.

microphysics is clearly evident as well as the high precipitation biases predicted by all experiments although CTRL and MPM2M are arguably within the observational error limits. The differential percentage relative to CTRL provides an additional measurement of the uncertainty arising from various microphysics treatments. The SNOTEL-site averages have the largest degree of sensitivity, and the domain averages display an intermediate sensitivity. The relatively weak microphysics dependency in the subdomain is a consequence of the opposite ridge–valley differentiations that tend to offset each other in the orographic region as shown in Fig. 6. (Recall that SNOTELs are typically deployed at local high altitudes.)

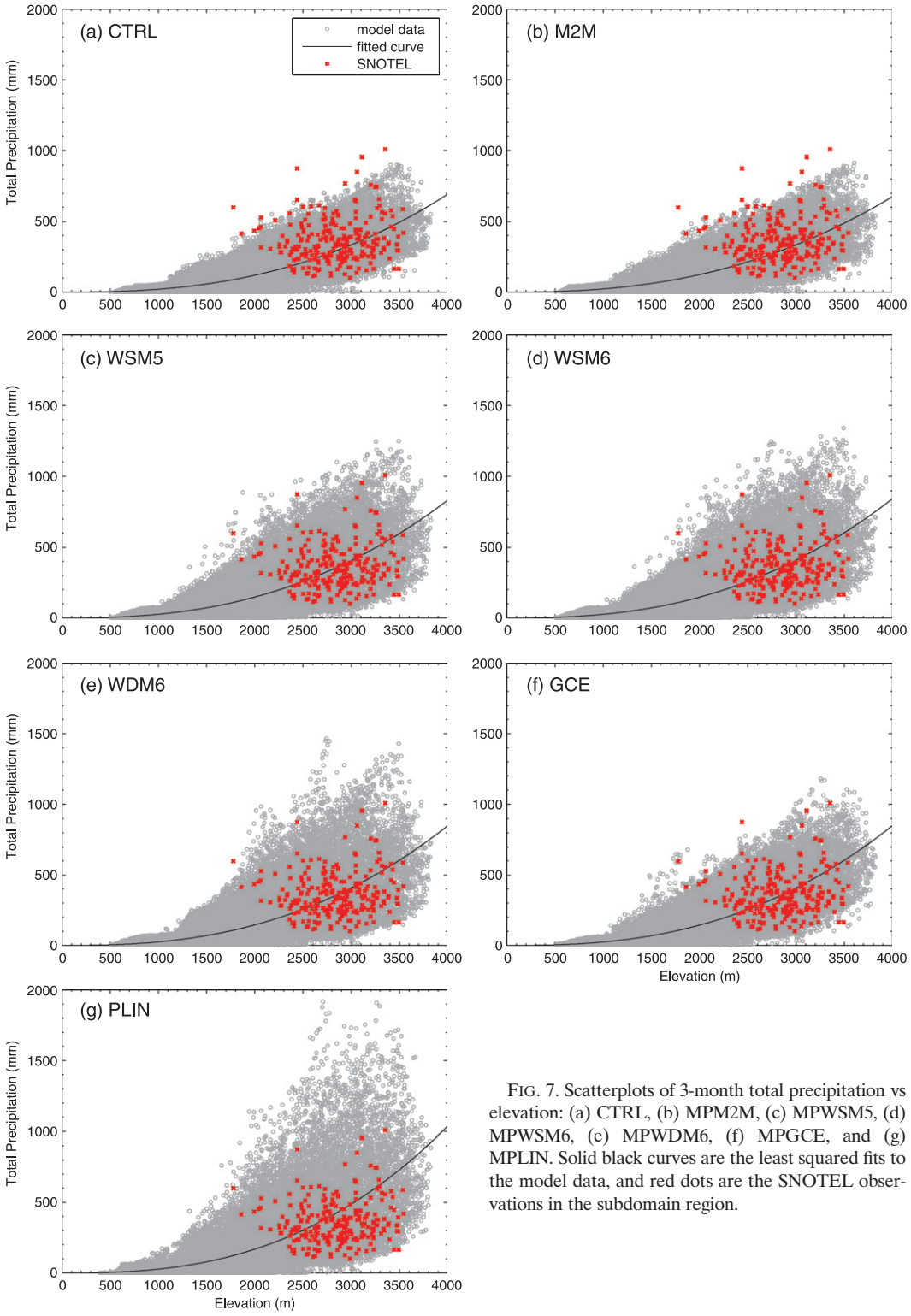

FIG. 7. Scatterplots of 3-month total precipitation vs elevation: (a) CTRL, (b) MPM2M, (c) MPWSM5, (d) MPWSM6, (e) MPWDM6, (f) MPGCE, and (g) MPLIN. Solid black curves are the least squared fits to the model data, and red dots are the SNOTEL observations in the subdomain region.

3) PRECIPITATION RATES

Both the precipitation occurrence and relative contribution to total amount rapidly decrease as the precipitation intensity increases in all simulations (not shown). Nevertheless, discernible differences exist among the parameterizations as shown in Fig. 8. It should be pointed out that herein the rain rate is derived from the archived

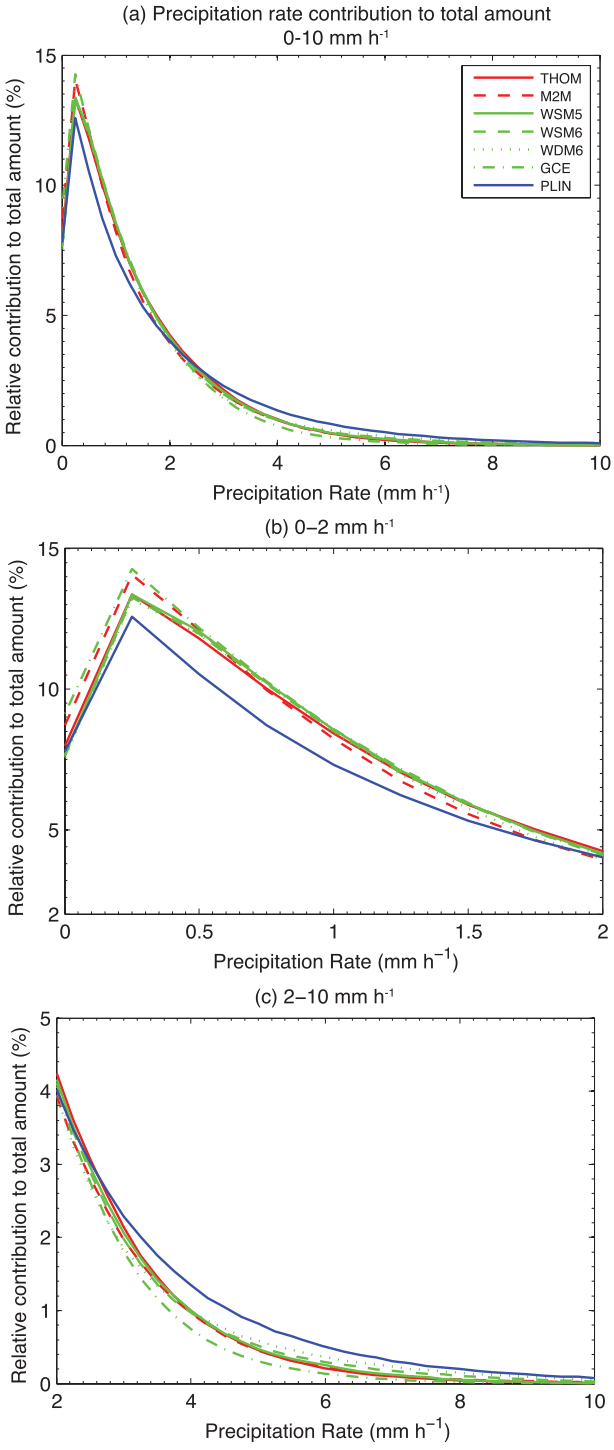

FIG. 8. (a) Relative contributions to total precipitation by different precipitation intensities in simulations using various microphysical parameterizations. (b) As in (a), but for precipitation rates from 0 to 2 mm h^{-1}. (c) As in (a), but for rates from 2 to 10 mm h^{-1}.

hourly accumulated precipitation data, rather than from the instantaneous intensity. GCE has the narrowest spectrum with the greatest portion of light precipitation below 1 mm h^{-1} and the smallest contribution from precipitation above 3 mm h^{-1}. In contrast, PLIN generates the widest spectrum with the largest (smallest) contribution from intense (light) precipitation. Other schemes display a similar pattern except for M2M, which gives rise to relatively more frequent weak precipitation events. Overall, these differentiations are not as significant as in warm-season convective precipitation (Liu and Moncrieff 2007).

4) CONDENSATE AND CLOUD AMOUNT

The subdomain averages of different hydrometeor species in Figs. 9 and 10 show considerable variability. First, cloud liquid water in CTRL and MPM2M is several times larger than cloud water in the W-series experiments. Second, the cloud ice variable in CTRL is distinctly less than all other parameterizations, but this is primarily due to predetermined definition of snow versus cloud ice by the scheme. Third, snow is the dominant category of all hydrometeors in all schemes except PLIN, in which graupel and snow have nearly equal amounts with less combined water content than any other experiment. The near absence of graupel in CTRL and MPM2M will be discussed later. It is perhaps not surprising that rain is minimal because of the deep winter low temperatures in the Colorado Headwaters region. The averages over the whole domain (not shown), albeit much smaller, feature the same basic profiles and differences among these parameterizations.

As shown in Fig. 10e, the total condensate contents (i.e., the sum of cloud water, rain, cloud ice, snow, and graupel) closely resemble each other in the upper troposphere except the comparatively larger cloud ice content in MPM2M (Fig. 9). The condensate profiles diverge more at lower levels. The maximum and minimum appear in GCE and PLIN, respectively, and differ by a factor of 3 at the surface. CTRL and MPM2M are relatively similar to each other below 2 km, while the three W-series experiments produce nearly the same condensate among this group. The significantly lower condensate aloft for the PLIN scheme coupled with the fact that it has the highest precipitation accumulation of all the schemes (Fig. 5) suggests that this scheme has a relatively high precipitation efficiency. The high fraction of relatively fast falling graupel (cf. snow) is consistent with this result (Fig. 10c).

When cloud fraction is computed by removing rain and graupel from the condensate data and assigning 100% cloudiness to grid boxes with more than 0.005 g kg^{-1}, then the average vertical profiles of cloud fraction are shown in

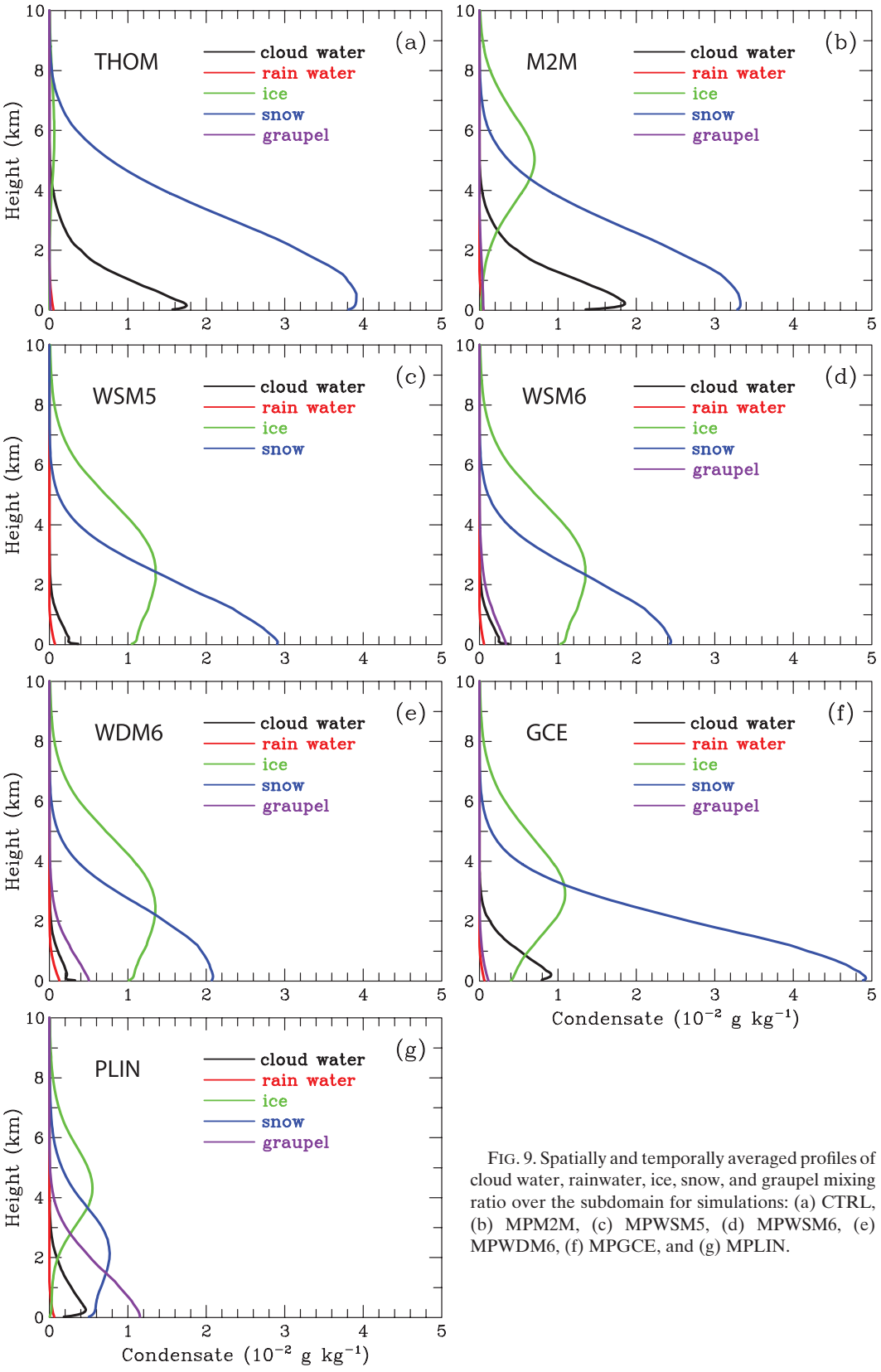

FIG. 9. Spatially and temporally averaged profiles of cloud water, rainwater, ice, snow, and graupel mixing ratio over the subdomain for simulations: (a) CTRL, (b) MPM2M, (c) MPWSM5, (d) MPWSM6, (e) MPWDM6, (f) MPGCE, and (g) MPLIN.

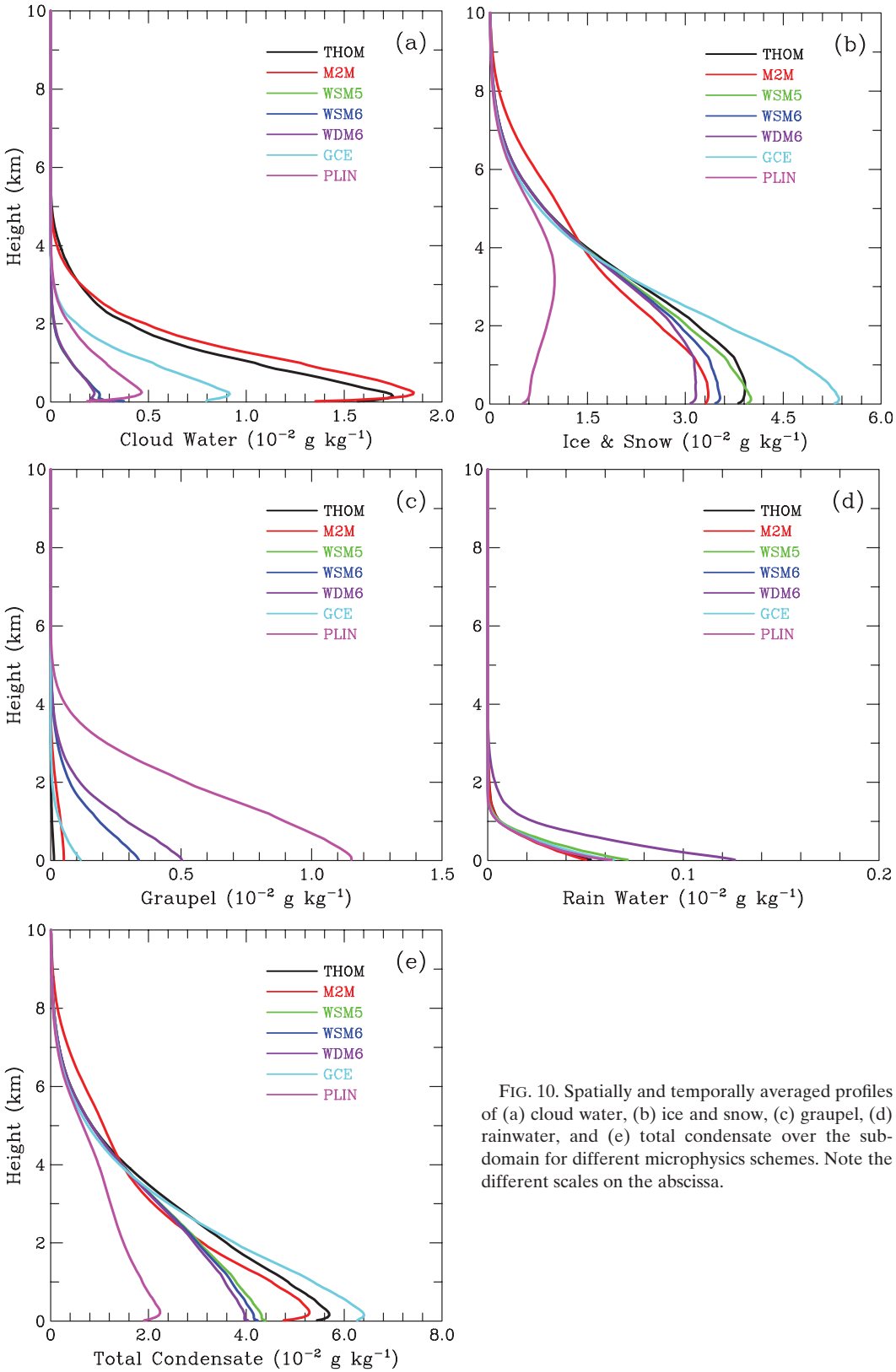

FIG. 10. Spatially and temporally averaged profiles of (a) cloud water, (b) ice and snow, (c) graupel, (d) rainwater, and (e) total condensate over the subdomain for different microphysics schemes. Note the different scales on the abscissa.

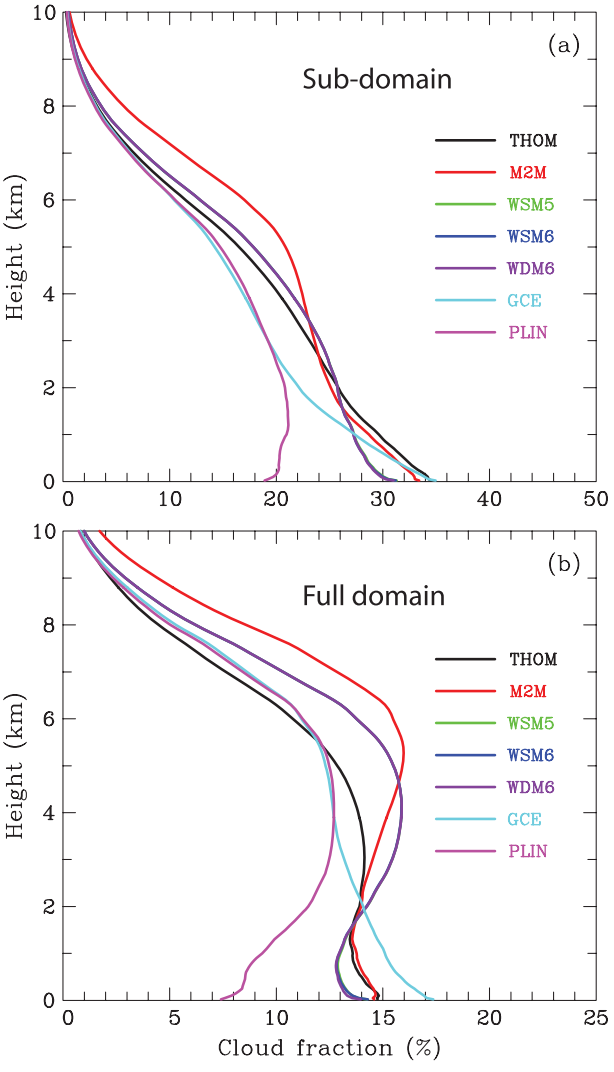

FIG. 11. Spatially and temporally averaged profiles of cloud fraction in simulations using different microphysics parameterizations for (a) the subdomain and (b) whole domain. Note that curves for three W-series schemes are mostly overlapped.

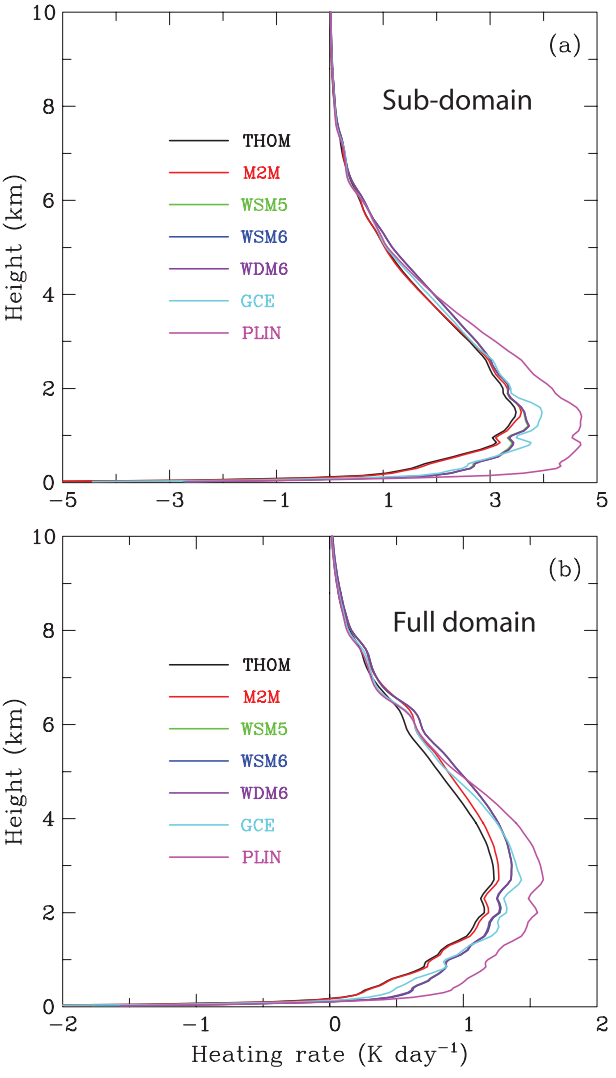

FIG. 12. As in Fig. 11, but for diabatic heating profiles.

Fig. 11. This calculation confirms that the MPM2M experiment predicts the most extensive high-level cloudiness, which might be worth deeper investigation by comparison to observed satellite data. All of the experiments correctly predict a greater fraction of low cloudiness due to the upslope forcing. Contradicting Fig. 10, the MPGCE experiment shows less cloud fraction at most levels than most other experiments, yet this experiment contains considerably more total condensate than the others. To explain this, either the rain and graupel are very small but nonzero at a large number of grid boxes, or there must be less numerous grid boxes with snow but a greater quantity of snow (Fig. 9f) in MPGCE than found in the other experiments.

5) LATENT HEATING

Diabatic heating in association with phase changes is an important energy source of large-scale atmospheric motions, which led us to investigate its sensitivity to microphysics treatment. The subdomain averages in Fig. 12a show a ground-based shallow cooling and an overlying deep warming in all experiments. Note that, unlike summertime convection (Liu and Moncrieff 2007), latent heating in winter storms is confined to much lower levels, consistent with the cloud structures presented above. Additionally, the near-surface cooling is much thinner than the warm-season counterpart as well as the distinct responsible physical processes, primarily evaporation and/or sublimation. Maximum heating occurs around 1.5 km, on average, with a value of ~3.5–4.7 K day^{-1}. MPLIN and CTRL generate the most and least warming, respectively,

and their difference is significant. As in other fields, the profiles in W series are almost completely overlapped, while MPM2M and CTRL experiments nearly match. Not surprisingly, the final precipitation amounts correlate very well to the diabatic heating with the MPLIN experiment producing the greatest heating and the largest precipitation amounts while the other experiments produce less of both. The domain means (Fig. 12b) display more elevated warming peaked at ~2–3 km, presumably due to less frequent but slightly thicker clouds over the flat areas surrounding the Rocky Mountains.

In essence, the latent heating contrast clearly indicates that the microphysics selection could significantly affect dynamical feedbacks of winter storms as they cross the Rockies and thus their subsequent evolutions. This issue warrants further research in the future.

6) DISCUSSION

The vertical distributions of hydrometeors in Figs. 9 and 10 cluster into four groups: 1) CTRL and MPM2M have high snow, high cloud water, and low graupel; 2) WSM5, WSM6, and WDM6 have moderate snow, low cloud water, and moderate graupel; 3) GCE has high snow, moderate cloud water, and low graupel; and 4) PLIN has low snow, low cloud water, and high graupel. These differences are quite remarkable considering that the vertical motions associated with storms over the complex terrain of the Rocky Mountains is typically less than 2 m s^{-1}. Perhaps most critical to matching the SNOTEL observations is the prediction of relatively high cloud water and low graupel as the schemes with least cloud water and most graupel stray the most from observations. At first glance one may conclude that different schemes' treatment of conversion of snow to graupel may be the dominant difference since highly rimed particles will deplete the cloud liquid water and produce graupel, which fall faster and likely increase the observed precipitation (Fig. 5). This factor plays an important role, however, other processes are also involved. The following is a partial list of factors: ice initiation, conversion pathways to graupel, the manner in which the schemes simulate the collection of snow and rain by graupel, and how snowfall speed is handled. The role of each of these factors in the observed differences between schemes is described below.

(i) Ice initiation

If a bulk scheme allows ice to initiate very near 0°C at ice saturation or above, then any additional water vapor will continue to grow the tiny crystals to snow size. This chain of events leads to removal of additional water vapor that could otherwise be available for the creation of cloud drops. Cloud droplets, in contrast to ice crystals and snow, float along with the wind and do not fall out as precipitation unless collected by falling hydrometeors. Thus, unphysical creation of ice crystals prematurely can lead to a higher precipitation efficiency than correct. Of the bulk parameterizations tested in this research, all except Thompson et al. (2008) and Morrison et al. (2009) are rapid to initiate ice from vapor when ice supersaturation is achieved or freeze water droplets prematurely, which is discussed in a subsequent subsection.

(ii) Graupel pathway: Snow riming

A very deliberate decision was made when developing the Thompson et al. (2008) scheme to evaluate critically each graupel production pathway. For instance, the efficiency of snow-collecting cloud water in nearly all past bulk schemes has been unity. While the efficiency under a wide range of conditions may be nearly 1, this is not always the case. The Thompson et al. (2008) and Morrison et al. (2009) schemes implemented a variable collection efficiency as a function of mean size of snow and cloud droplets following Wang and Ji (2000).

In addition, more care must be taken when coding because a moderate amount of snow passing through a very small amount of cloud water probably does not immediately result in a spherical hydrometeor with a density half that of frozen ice (note that most schemes assume graupel density of 400 kg m^{-3}). Rather, the snow collects a few tiny droplets and simply adds the mass into a particle that remains very snowlike. If, however, a bulk scheme follows the various treatments of this process based on Lin et al. (1983) or Rutledge and Hobbs (1984), then the likely result is to create graupel, which will boost the particle density by a factor of 4 and fall twice as quickly as a snowflake. In contrast, the Thompson scheme very conservatively converts only partial amounts of combined snow and cloud water into graupel, while retaining 5%–75% of the mass in the original category.

(iii) Graupel pathway: Freezing of rain

Another graupel pathway is the freezing of rain. Many of the bulk schemes claim to use the same method introduced by Bigg (1953), which is in error in all except the Thompson scheme. The proper reference by all other schemes should be Wisner et al. (1972) who claimed to implement the Bigg (1953) scheme's temperature and volume dependence of drops freezing. However, the Wisner adaptation to a distribution of drops is not consistent with a strict bin-model approach. In contrast, the Thompson scheme deliberately implemented and stored results from a discretization of water droplet bins in a lookup table to match the true method of Bigg (1953).

(iv) Graupel pathway: Collisions of graupel and snow

Though not necessarily the most efficient way to produce graupel, bulk schemes based on Lin et al. (1983) almost always include a term for graupel to collect snow. The collection of snow by graupel (or hail) was assigned a temperature-dependent efficiency in Lin et al. (1983) and constant value of 10% in Rutledge and Hobbs (1984), yet almost no one has considered its ramifications or whether it makes any sense physically. We submit that graupel hardly ever collides with and collects snow. One author of this paper has photographed snow crystals for nearly a decade and has never observed such a particle on the ground. If collisions between these two particles resulted in collection 10% of the time, observing a graupel particle with an attached snowflake would be commonplace. The modeling study by Lin and Colle (2009) shows how unrealistic graupel growth in a model can be with this process active, and also the sensitivity testing by Jankov et al. (2009) reveals that disregarding the accretion of snow by graupel reduced the precipitation overestimation ~50%. Our own test shutting off this production term for graupel caused only a small change to 10-day precipitation amount, but it caused a massive decrease (increase) in graupel (snow) aloft.

(v) Graupel pathway: Collisions of rain and snow

Rain and snow collisions are probably the most efficient creator of graupel. This seems logical if we consider a hypothetical 1-mm diameter raindrop falling at 7 m s^{-1} colliding with a 0.5-mm snowflake that instantly initiates the freezing process and unifies the resulting 2 particles. The trouble arises with implementation details and engineering decisions, or lack thereof. Similar to snow collecting cloud water, there may be times when a very large size snow particle collects very small raindrops. Should the resulting particle be immediately assumed to fit the category of graupel? For the most part, the Lin-based schemes have 100% capture if geometric collision between rain and snow is possible and they always result in graupel production. Furthermore, the mathematical shortcut of either Wisner et al. (1972) or Mizuno (1990) has been applied for decades rather than more advanced solutions by Verlinde et al. (1990) or Gaudet and Schmidt (2005). The Thompson scheme decided once again to implement a direct bin-model approach and store the results in a lookup table for application during the simulation.

(vi) Graupel pathway: Collisions of rain and graupel

Similar to rain colliding with snow, rain and graupel collisions typically implement the Mizuno (1990) shortcut, which is a far worse solution in this case than it is for rain/snow collisions. This is due to the more frequent occurrence of similar fall speeds between the two species in which the mathematical simplifications of removing the terminal velocity difference outside of the integral over diameter is a violation of proper mathematics.

(vii) Snowfall speed

Finally, the terminal velocity constants used in the ARW-WRF MP-Lin scheme are explicitly stated in the Locatelli and Hobbs (1974) to refer to a particle description of ''graupel-like snow of hexagonal type.'' So, in effect, the snow category in the Lin scheme is using terminal velocities somewhat appropriate of graupel. Lin and Colle (2009) show that this fall speed relation characterizes snow as mostly falling faster than 2 m s^{-1}, whereas observations show roughly half that speed.

The above discussion shows how numerous small improvements to a physical parameterization can combine to produce a superior overall result. These small improvements, in turn, were implemented through careful consideration of how the parameterization handles realistic physical processes using high-resolution aircraft and ground observations as a guide (Thompson et al. 2004, 2008).

c. Sensitivity to LSMs

Three LSMs suitable for long-range simulations were compared: (i) Noah LSM, a four-layer soil temperature and moisture model with canopy moisture and snow and frozen soil physics (Chen and Dudhia 2001); (ii) RUC LSM, a six-layer soil temperature and moisture model with multilayer snow and frozen soil physics (Smirnova et al. 2000); and (iii) Pleim–Xiu LSM, a two-layer force-restore soil temperature and moisture model (Pleim and Xiu 1995; Xiu and Pleim 2001). These schemes were employed in CTRL, LSRUC, and LSPX and LSPX2, respectively (Table 1). LSPX and LSPX2 differ in the choice of surface layer and PBL physics. Experiment LSPX2 was primarily motivated by the question of whether the performance would be improved when a set of Pleim–Xiu surface layer, boundary layer, and land surface parameterizations is used. The comparison in the two Pleim–Xiu series can also be used to evaluate how the overlying surface layer and PBL treatments affect the LSM performance.

For the most part, model results have a much weaker dependence on the choice of LSMs than on cloud microphsysics as demonstrated in accumulative precipitation (Fig. 13). All LSMs overpredict the accumulation, mostly arising from the discrepancy during three heavy snowfall episodes in January and February. As indicated in Table 2, the bias in 3 LS series becomes more than 10% over the SNOTEL sites, worse than CTRL. The variation in precipitation totals for both the subdomain and whole domain is less than 10% when the Noah LSM is replaced

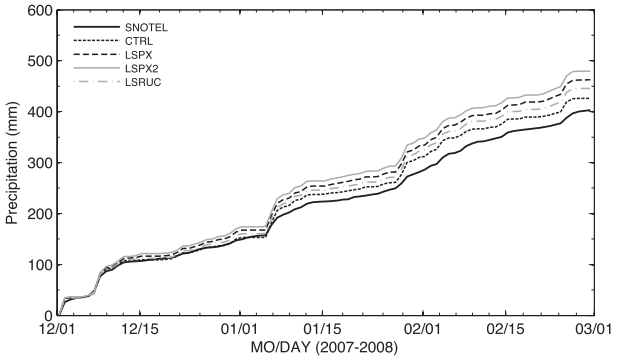

FIG. 13. Evolution of accumulated precipitation averaged over SNOTEL sites for simulations using various land surface models.

with either the RUC LSM or Pleim–Xiu LSM (Table 2). The largest precipitation change occurs in LSPX2, accounting for the combined effects of different surface layer, PBL, and LSM treatments. The best agreement with SNOTEL data may indicate that Noah LSM is an optimal option for cold-season snowfall simulations in this orographic region.

The differential accumulation in Fig. 14 illustrates the influence of LSMs on spatial distributions. The difference from CTRL is below 20 mm at majority of grid points and is much smaller than the changes in association with various microphysics schemes (Fig. 6). Both RUC and Pleim–Xiu LSMs tend to reduce precipitation in the eastern Utah and northern Arizona and enhance precipitation over most of the headwaters area and east of the Rockies, but the former is comparatively closer to Noah LSM than the latter. The ratio of grid boxes with a positive and negative precipitation deviation relative to CTRL is 3.7, 3.5, and 2.4 for LSRUC, LSPX, and LSPX2, respectively.

Because LSMs directly affect surface features, it is therefore of interest to compare some surface fields in these schemes. In general, the difference is trivial in the areal average daily fluctuations of wind speed and thermodynamics as well as surface fluxes (not shown). The most notable is the headwaters temperature, which in CTRL is relatively colder than in other simulations.

d. Sensitivity to PBL schemes

A total of six PBL parameterizations were tested: (i) Mellor–Yamada–Janjic (MYJ) local mixing turbulent kinetic energy (TKE) scheme (Janjic 2002), (ii) Yonsei University (YSU) nonlocal-K scheme (Hong et al. 2006), (iii) Quasi-Normal Scale Elimination (QNSE) TKE scheme (Sukoriansky et al. 2005), (iv) Mellor–Yamada–Nakanishi–Niino level-2.5 (MYNN) TKE scheme (Nakanishi and Niino 2006), (v) Mellor–Yamada–Nakanishi–Niino level-3 (MYNN3) TKE scheme

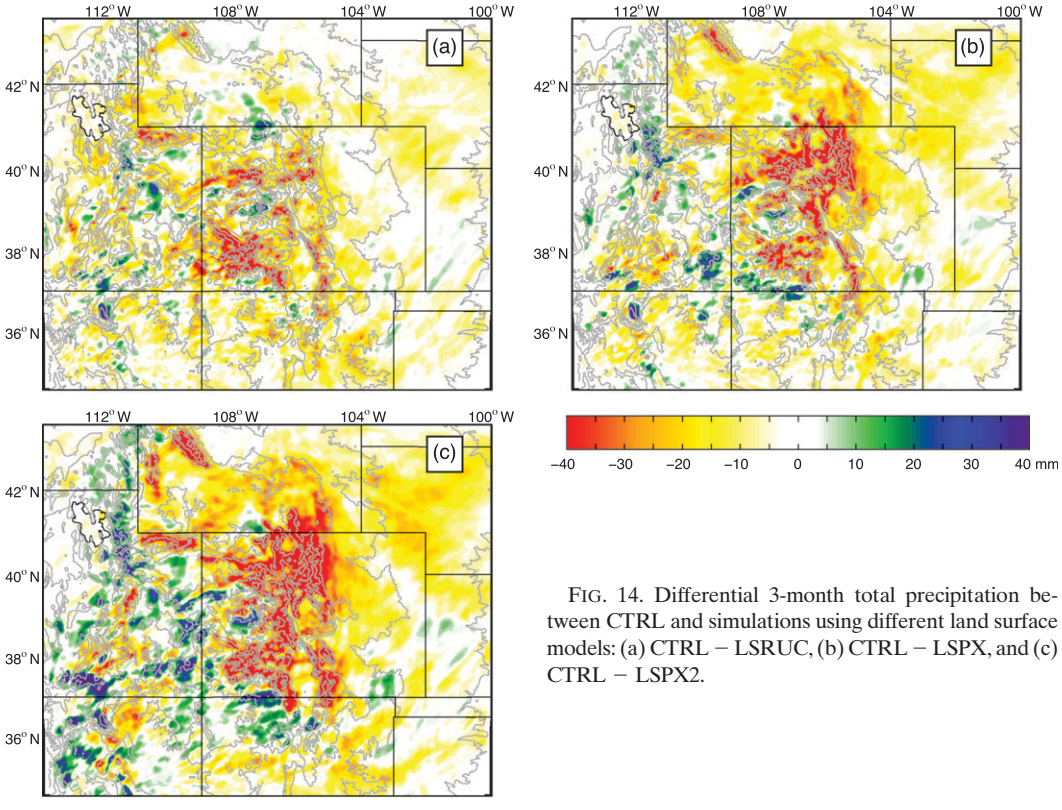

FIG. 14. Differential 3-month total precipitation between CTRL and simulations using different land surface models: (a) CTRL − LSRUC, (b) CTRL − LSPX, and (c) CTRL − LSPX2.

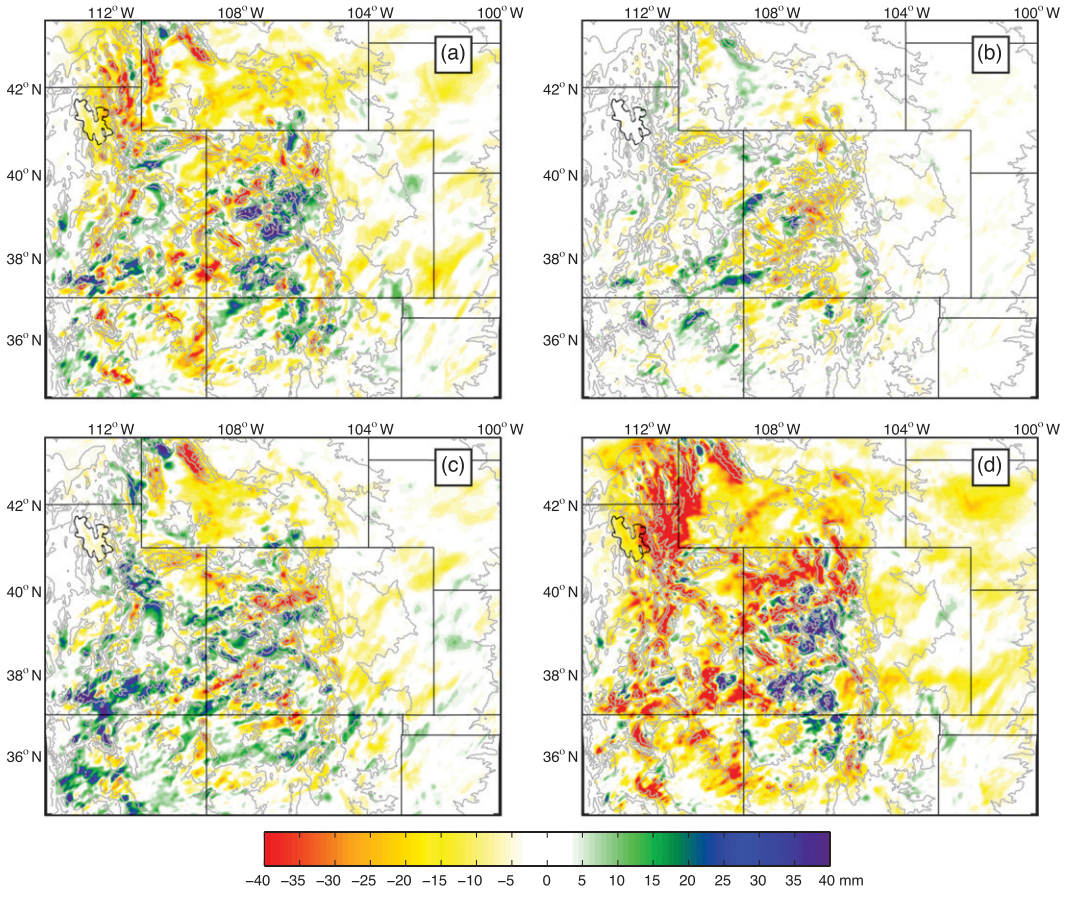

FIG. 15. Differential 3-month total precipitation between CTRL and simulations using different PBL parameterizations: (a) CTRL − BLYSU, (b) CTRL − BLQNSE, (c) CTRL − BLMYNN3, and (d) CTRL − BLBL.

(Nakanishi and Niino 2006), and (vi) Bougeault–Lacarrere (BL) TKE scheme (Bougeault and Lacarrere 1989). They were applied in experiments CTRL, BLYSU, BLQNSE, BLMYNN, BLMYNN3, and BLBL, respectively (Table 1). Because some PBL schemes only work with a specific surface layer scheme, different surface layer parameterizations have been utilized in these simulations and thus might complicate the sensitivity assessment.

Precipitation accumulations in the headwaters are largely insensitive to the choice of PBL parameterizations as evidenced by the minimal variations of accumulated precipitation in Table 2. The differentiation from CTRL is small in all three averages with an only exception for the whole-domain average in BLBL. As shown in Fig. 15, the accumulative precipitation difference is most evident in high mountains and exhibits a similar level of sensitivity to LSMs. (Because of the great similarity between BLMYNN and BLMYNN3, only the latter is presented.) Visually, it seems that QNSE is closest to MYJ. The largest domain-mean difference from CTRL appears in BLBL. QNSE generates a slightly greater precipitation over most of the headwaters, whereas a lighter (heavier) precipitation prevails in the southern and central (northern) headwaters for YSU and BL. As for the two MYNN schemes, weaker and stronger precipitation accumulation dominates in the southwestern portion and northern and eastern parts of the model domain, respectively.

Surface fields (not shown) are insensitive to the PBL treatment, too, implying a rather weak coupling between the PBL and surface processes in the cold headwaters. One discernible difference is the somewhat warmer and windier conditions in BLBL than in other simulations.

e. Sensitivity to radiation schemes

Two sophisticated radiation schemes suitable for multimonth integrations were chosen for our sensitivity study: (i) the NCAR CAM radiative transfer model for both longwave and shortwave radiation (Collins et al. 2004), and (ii) an updated version of Rapid Radiative Transfer Model (RRTM; Mlawer et al. 1997), corresponding to experiments CTRL and RRTMG, respectively (Table 1). The areal means (Table 2) are trivially affected by radiation

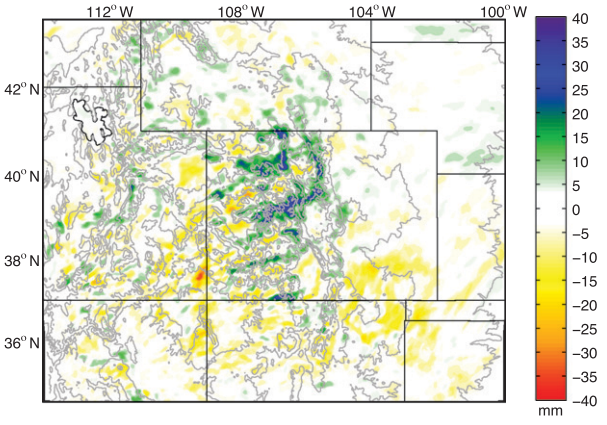

FIG. 16. Differential 3-month total precipitation between CTRL and RRTMG.

parameterizations. The regional accumulation difference between this pair of simulations (Fig. 16) is quite small, even smaller than the counterparts in both the LS series and BL series, suggesting the least radiation dependency. On average, CAM generates a slightly stronger radiative cooling at most levels than RRTMG (not shown).

4. Summary

Because of the large variety of parameterizations for cloud microphysics, land surface processes, planetary boundary layer physics, and radiative processes, an important question is how the high-resolution regional climate simulations rely on these physical schemes. This study investigated the sensitivity of winter season snowfall in the Colorado Headwaters to 7 bulk microphysics parameterizations, 3 LSMs, 6 PBL parameterizations, and 2 radiative transfer models by performing a series of 3-month simulations with a 4-km grid spacing. The selected period spanned 1 December 2007–29 February 2008, corresponding to an above-average snowfall (wet) season in the Colorado Rocky Mountains. The model results were evaluated with available SNOTEL observations. In addition to assessing the uncertainty related to the choice of various physical schemes, the results may guide future improvement and development of these parameterizations and aid the selection of adequate parameterizations for the regional modeling community. Our major findings are summarized as follows:

- Irrespective of the physical scheme selection, the regional climate model can reasonably reproduce the observed daily snowfall fluctuation patterns, in particular the heavy snowfall events associated with significant synoptic weather systems, and ridge–valley spatial distributions. This result is presumably attributable to proper depiction of the complex topography in the high-resolution model as well as the realistic large-scale forcing provided by the NARR data.
- Simulation of winter snowfall in this region with complex terrain is most sensitive to cloud microphysics treatments. The Thompson et al. (2008) and Morrison et al. (2009) bulk microphysics schemes have comparable skill and are apparently superior to other schemes that substantially overforecasted the snowfall amount. The excessive snowfall prediction is most problematic in the Chen and Sun (2002) scheme directly based on Lin et al. (1983).
- The comparisons show only a moderate-to-weak dependency on land surface, planetary boundary layer, and radiation parameterizations. The weak sensitivity largely results from the weak land surface coupling, shallow PBL development, and its small diurnal variability, all of which, in turn, are related to weak solar radiative heating in the winter. Nevertheless, LSMs and PBL treatments still have nonnegligible impacts on detailed spatial distributions of surface precipitation.

An identical set of physical parameterizations as in CTRL has been employed in six-month precipitation simulations for four past cold seasons (Ikeda et al. 2010). Nevertheless, the above conclusions are obtained from experimentations over a specific region, and therefore may not be exclusively applicable to other geographical locations. Furthermore, the results derived from cold-season snowfall simulations may not be generally applicable to warm-season convective precipitation. Additionally, in the warm-season active land–atmosphere energy exchanges and solar heating likely lead to a comparable level of sensitivity among the cloud microphysics, land surface physics, PBL processes, and radiations.

This study is aimed at assessing the physical parameterization dependency of orographic snowfall simulations in a high-resolution regional climate model, but a detailed interpretation of the results is beyond the scope of the current paper. In view of the high sensitivity to cloud microphysics, however, a systematic examination of critical physical processes accounting for the precipitation and cloud differences among the tested parameterizations is needed, for example, based on idealized simulations and intensive field programs.

Acknowledgments. This work is supported by the NSF-supported Water System program at NCAR.

REFERENCES

Bigg, E. K., 1953: The supercooling of water. *Proc. Phys. Soc. London,* **66B,** 688–694.

Bougeault, P., and P. Lacarrere, 1989: Parameterization of orography-induced turbulence in a mesobeta-scale model. *Mon. Wea. Rev.,* **117,** 1872–1890.

Chen, F., and J. Dudhia, 2001: Coupling an advanced land surface-hydrology model with the Penn State–NCAR MM5 modeling system. Part I: Model implementation and sensitivity. *Mon. Wea. Rev.,* **129,** 569–585.

Chen, S.-H., and W.-Y. Sun, 2002: A one-dimensional time dependent cloud model. *J. Meteor. Soc. Japan,* **80,** 99 118.

Colle, B. A., and C. F. Mass, 2000: The 5–9 February 1996 flooding event over the Pacific Northwest: Sensitivity studies and evaluation of the MM5 precipitation forecasts. *Mon. Wea. Rev.,* **128,** 593–617.

——, K. J. Westrick, and C. F. Mass, 1999: Evaluation of MM5 and Eta-10 precipitation forecasts over the Pacific Northwest during the cool season. *Wea. Forecasting,* **14,** 137–154.

——, C. F. Mass, and K. J. Westrick, 2000: MM5 precipitation verification over the Pacific Northwest during the 1997–99 cool seasons. *Wea. Forecasting,* **15,** 730–744.

——, Y. Lin, S. Medina, and B. F. Smull, 2008: Orographic modification of convection and flow kinematics by the Oregon coast range and cascades during IMPROVE-2. *Mon. Wea. Rev.,* **136,** 3894–3916.

Collins, W. D., and Coauthors, 2004: Description of the NCAR Community Atmosphere Model (CAM3.0). NCAR Tech. Note NCAR/TN-464+STR, 226 pp.

Garvert, M. F., B. A. Colle, and C. F. Mass, 2005: The 13–14 December 2001 IMPROVE-2 event. Part I: Synoptic and mesoscale evolution and comparison with a mesoscale model simulation. *J. Atmos. Sci.,* **62,** 3474–3492.

Gaudet, B. J., and J. M. Schmidt, 2005: Assessment of hydrometeor collection rates from exact and approximate equations. Part I: A new approximate scheme. *J. Atmos. Sci.,* **62,** 143–159.

Grubišić, V., R. K. Vellore, and A. W. Huggins, 2005: Quantitative precipitation forecasting of wintertime storms in the Sierra Nevada: Sensitivity to the microphysical parameterization and horizontal resolution. *Mon. Wea. Rev.,* **133,** 2834–2859.

Hong, S.-Y., and J.-O. J. Lim, 2006: The WRF Single-Moment 6-Class Microphysics Scheme (WSM6). *J. Korean Meteor. Soc.,* **42,** 129–151.

——, Y. Noh, and J. Dudhia, 2006: A new vertical diffusion package with an explicit treatment of entrainment processes. *Mon. Wea. Rev.,* **134,** 2318–2341.

Ikeda, K., and Coauthors, 2010: Simulation of seasonal snowfall over Colorado. *Atmos. Res.,* **97,** 462–477.

Janjic, Z. I., 2002: Nonsingular implementation of the Mellor–Yamada level 2.5 scheme in the NCEP Meso model. NCEP Office Note 437, 61 pp.

Jankov, I., J.-W. Bao, P. J. Neiman, P. J. Schultz, H.-L. Yuan, and A. B. White, 2009: Evaluation and comparison of microphysical algorithms in ARW-WRF model simulations of atmospheric river events affecting the California coast. *J. Hydrometeor.,* **10,** 847–870.

——, P. J. Schultz, C. J. Anderson, and S. E. Koch, 2007: The impact of different physical parameterizations and their interactions on cold season QPF in the American River basin. *J. Hydrometeor.,* **8,** 1141–1151.

Leung, L. R., and Y. Qian, 2003: The sensitivity of precipitation and snowpack simulations to model resolution via nesting in regions of complex terrain. *J. Hydrometeor.,* **4,** 1025–1043.

Lim, K.-S. S., and S.-Y. Hong, 2010: Development of an effective double-moment cloud microphysics scheme with prognostic cloud condensation nuclei (CCN) for weather and climate models. *Mon. Wea. Rev.,* **138,** 1587–1612.

Lin, Y., and B. A. Colle, 2009: The 4–5 December 2001 IMPROVE-2 event: Observed microphysics and comparisons with the Weather Research and Forecasting model. *Mon. Wea. Rev.,* **137,** 1372–1392.

Lin, Y.-L., R. D. Farley, and H. D. Orville, 1983: Bulk parameterization of the snow field in a cloud model. *J. Climate Appl. Meteor.,* **22,** 1065–1092.

Liu, C.-H., and M. W. Moncrieff, 2007: Sensitivity of cloud-resolving simulations of warm-season convection to cloud microphysics parameterizations. *Mon. Wea. Rev.,* **135,** 2854–2868.

Locatelli, J. D., and P. V. Hobbs, 1974: Fall speeds and masses of solid precipitation particles. *J. Geophys. Res.,* **79,** 2185–2197.

Mesinger, F., and Coauthors, 2006: North American regional reanalysis. *Bull. Amer. Meteor. Soc.,* **87,** 343–360.

Milbrandt, J. A., M. K. Yau, J. Mailhot, S. Belair, and R. McTaggart-Cowan, 2010: Simulation of an orographic precipitation event during IMPROVE-2. Part II: Sensitivity to the number of moments in the bulk microphysics scheme. *Mon. Wea. Rev.,* **138,** 625–642.

Mizuno, H., 1990: Parameterization of the accretion process between different precipitation elements. *J. Meteor. Soc. Japan,* **68,** 395–398.

Mlawer, E. J., S. J. Taubman, P. D. Brown, M. J. Iacono, and S. A. Clough, 1997: Radiative transfer for inhomogeneous atmospheres: RRTM, a validated correlated-k model for the longwave. *J. Geophys. Res.,* **102** (D14), 16 663–16 682.

Morrison, H., G. Thompson, and V. Tatarskii, 2009: Impact of cloud micrpohysics on the development of trailing stratiform precipitation in a simulated squall line: Comparison of one- and two-moment schemes. *Mon. Wea. Rev.,* **137,** 991–1007.

Nakanishi, M., and H. Niino, 2006: An improved Mellor-Yamada level-3 model: Its numerical stability and application to a regional prediction of advection fog. *Bound.-Layer Meteor.,* **119,** 397–407.

Pleim, J. E., and A. Xiu, 1995: Development and testing of a surface flux and planetary boundary layer model for application in mesoscale models. *J. Appl. Meteor.,* **34,** 16–32.

Rasmussen, R. J., and Coauthors, 2011: High-resolution coupled climate runoff simulations of seasonal snowfall over Colorado: A process study of current and warmer climate. *J. Climate,* **24,** 3015–3048.

Rasmussen, R. M., and Coauthors, 2001: Weather Support to Deicing Decision Making (WSDDM): A winter weather nowcasting system. *Bull. Amer. Meteor. Soc.,* **82,** 579–595.

Reisner, J., R. J. Rasmussen, and R. T. Bruintjes, 1998: Explicit forecasting of supercooled liquid water in winter storms using the MM5 mesoscale model. *Quart. J. Roy. Meteor. Soc.,* **124B,** 1071–1107.

Rutledge, S. A., and P. V. Hobbs, 1984: The mesoscale and microscale structure and organization of clouds and precipitation in midlatitude cyclones. XII: A diagnostic modeling study of precipitation development in narrow cold-frontal rainbands. *J. Atmos. Sci.,* **41,** 2949–2972.

Serreze, M. C., M. P. Clark, R. L. Armstrong, D. A. McGinnis, and R. S. Pulwarty, 1999: Characteristics of the western United States snowpack from snowpack telemetry (SNOTEL) data. *Water Resour. Res.,* **35,** 2145–2160.

——, ——, and A. Frei, 2001: Characteristics of large snowfall events in the montane western United States as examined using snowpack telemetry (SNOTEL) data. *Water. Resour. Res.,* **37,** 675–688.

Skamarock, W. C., and Coauthors, 2008: A description of the advanced research WRF version 3. NCAR Tech. Note NCAR/TN-475+STR, 113 pp.

Smirnova, T. G., J. M. Brown, S. G. Benjamin, and D. Kim, 2000: Parameterization of cold-season processes in the MAPS land-surface scheme. *J. Geophys. Res.,* **105** (D3), 4077–4086.

Sukoriansky, S., B. Galperin, and V. Perov, 2005: Application of a new spectral theory of stably stratified turbulence to the atmospheric boundary layer over sea ice. *Bound.-Layer Meteor.,* **117,** 231–257.

Tao, W.-K., and J. Simpson, 1993: The Goddard Cumulus Ensemble model: Part I. Model description. *Terr. Atmos. Oceanic Sci.,* **4,** 19–54.

Thompson, G., R. M. Rasmussen, and K. Manning, 2004: Explicit forecasts of winter precipitation using an improved bulk microphysics scheme. Part I: Description and sensitivity analysis. *Mon. Wea. Rev.,* **132,** 519–542.

——, P. R. Field, W. R. Hall, and R. M. Rasmussen, 2008: Explicit forecasts of winter precipitation using an improved bulk microphysics scheme. Part II: Implementation of a new snow parameterization. *Mon. Wea. Rev.,* **136,** 5095–5115.

Verlinde, J., P. J. Flatau, and W. R. Cotton, 1990: Analytical solutions to the collection growth equation: Comparison with approximate methods and application to the cloud micro- physics parameterization schemes. *J. Atmos. Sci.,* **47,** 2871–2880.

Wang, P. K., and W. Ji, 2000: Collision efficiencies of ice crystals at low-intermediate Reynolds numbers colliding with supercooled cloud droplets: A numerical study. *J. Atmos. Sci.,* **57,** 1001–1009.

Wisner, C., H. D. Orville, and C. Myers, 1972: A numerical model of a hail-bearing cloud. *J. Atmos. Sci.,* **29,** 1160–1181.

Xiu, A., and J. E. Pleim, 2001: Development of a land surface model. Part I: Application in a mesoscale meteorology model. *J. Appl. Meteor.,* **40,** 192–209.

Yang, D., B. E. Goodison, J. R. Metcalfe, V. S. Golubev, R. Bates, T. Pangburn, and C. L. Hanson, 1998: Accuracy of NWS 8″ standard nonrecording precipitation gauge: Results and application of WMO intercomparison. *J. Atmos. Oceanic Technol.,* **15,** 54–68.